Alternating Tangent Approach for the Optimal Vulcanization of 2D-3D EPM/EPDM Thick Elements

G. Milani,[1] F. Milani[2]

[1]*Dipartimento di Ingegneria Strutturale (DIS), Politecnico di Milano, Piazza Leonardo da Vinci 32, 20133, Milano, Italy*
[2]*CHEM.CO Consultant, Via J.F.Kennedy 2, Occhiobello, Rovigo 45030, Italy*

Received 30 March 2009; accepted 28 July 2009
DOI 10.1002/app.31239
Published online 7 October 2009 in Wiley InterScience (www.interscience.wiley.com).

ABSTRACT: The main problem in industrial practice when dealing with the curing process of thick EPM/EPDM elements is constituted by the different temperatures, which undergo internal (cooler) and external regions. Indeed, while internal layers remain essentially under-vulcanized, external coating is always over-vulcanized, resulting in an overall average tensile strength insufficient to permit the utilization of the items in several applications where it is required a certain level of performance. A possibility to improve rubber output mechanical properties is the utilization of mixtures of at least two peroxides, the first highly active at high temperatures (i.e., for external layers), the second at low temperatures (internal regions). In this framework, in this article, a simple numerical procedure for the optimization of final mechanical properties of vulcanized 2D and 3D thick rubber items is presented. In particular, a so called alternating tangent approach (AT) for the determination of the optimal input parameters to use during the production of complex 2D/3D thick items is presented. Vulcanization external temperature T_c and rubber exposition time t are assumed as input production parameters, whereas output mechanical property to optimize is represented by the average tensile strength of the item. In the algorithm, a sufficiently large interval of exposition times at fixed T_c (or curing temperatures at fixed exposition times) is chosen at the initial iteration, namely evaluating rubber tensile strength at a very under-vulcanized and at a very over-vulcanized exposition time. For each extreme of the interval, first derivatives of final tensile strength with respect to exposition time (or curing temperature) are evaluated numerically. At the successive iteration, search exposition interval is reduced to one-half through bisection, selecting the right or left semi-interval basing the choice on first derivative sign evaluated at the middle point. The approach proposed converges very quickly to the optimal solution, competing favorably both with a very expensive method based on the subdivision of the domain in a refined grid of points and with recently presented GA approaches. Two meaningful examples of engineering interest, consisting of an high voltage electric cable and a 3D thick rubber docks bumper are illustrated. When dealing with the 3D item, due to its thickness, different mixtures of two peroxides (50%-50%, 25%-75% and 75%-25% molar ratios) are also used to improve drastically final mechanical properties. Optimal production T_c and t parameters are obtained for all the cases analyzed. J Appl Polym Sci 115: 1995–2012, 2010

Key words: EPM/EPDM elastomers; vulcanization; optimization; Fourier's heat transmission law

INTRODUCTION

EPM/EPDM elastomers are used in engineering practice in a wide range of applications, including e.g. high/medium voltage power cables insulation, weather strips, docks bumpers, etc.

An increasing penetration of EPM/EPDM into the cross-linked polyethylene (XLPE) market share is expected by the majority of producers in the next few years, due to the increasing need of utilizing polymeric items at relatively high temperatures. As well known, in fact, XLPE hardly matches such increasing restricting requirements, due to its dimensional stability problems at temperatures above 90°C.

On the other hand, in several cases of industrial interest, a threshold value of *a-priori* established rubber output mechanical properties (e.g. tensile strength, tear resistance, etc.) is required, to avoid premature failures and/or insufficient performance.

Unfortunately, EPM/EPDM producers are usually unable to guarantee a good and homogeneous degree of vulcanization in presence of thick rubber elements, a quite important drawback strictly connected to the fact that external rubber layers undergo temperature profiles totally different with respect to the internal ones. This matter implies the impossibility to utilize thick rubber items in applications where it is required a high level/high quality mechanical performance of the product.

Such problem is particularly important, for instance, for high voltage electric cables, where insulator thicknesses exceed 1 cm.

In all these cases, the overall vulcanization level becomes much more complicated to predict and

Correspondence to: G. Milani (gabriele.milani@polimi.it).

the development of a numerical model able to give to practitioners information on the most suitable production parameters to adopt becomes a key issue.

In this framework, in this article, a numerical model able both to (1) predict temperature profiles for each point of a generic 3D rubber item subjected to vulcanization and to (2) furnish an estimation of EPM/EPDM average mechanical properties expected at the end of the production process is presented. At present, only unsophisticated and heuristic numerical models based on finite differences and suitable to analyzed only axi-symmetric problems (see for instance[1-5]) are available in the literature.

Here, Fourier's heat equation in its general 3D form is used for the determination through finite elements (FEM) of temperature profiles for complex rubber 3D items obtained by extrusion, compression, and injection molding.

Rubber tensile strength is monitored as output quantity to optimize. Nevertheless, it is stressed that the approach proposed is aimed at selecting any output mechanical property as optimization objective function, meaning that the procedure could be used by manufactures in a general framework and without any conceptual difficulty.

A fundamental parameter, which enters into the optimization process, is the relation among half-life of peroxides used for cross-linking process ($t_{1/2}$), temperature of each point of the item during the heating process and mechanical properties of rubber as a function of unreacted peroxide.

In particular, several questions arise from the previous aspects, related to the fact that experimental evidences show[6–8] that rubber mechanical properties (e.g. tensile strength, elongation, tear resistance, etc.) depend nonlinearly on the unreacted peroxide concentration C_i. More in detail, for high values of C_i, rubber results not vulcanized with a very low tensile/tear strength, whereas for lower values of C_i, experience shows that an optimal concentration $\overline{C}_i$ exists where output mechanical properties reach their maximum. Exceeded this optimal concentration, the item passes in the over-vulcanized region with a slight decrease of mechanical properties.

In this framework, a new simple alternating tangent approach (AT) based on a bisection procedure is proposed for the maximization of rubber mechanical properties.

Vulcanization external temperature T_c and rubber exposition time t are assumed as input production parameters, whereas output mechanical property to optimize is represented by the average tensile strength of the item.

In the algorithm, a sufficiently large interval of exposition times at fixed T_c (or alternatively a T_c interval at fixed t) is chosen at the initial iteration and rubber tensile strength is evaluated at the interval extremes (i.e., a very under-vulcanized and at a very over-vulcanized exposition time). First derivatives of final tensile strength with respect to exposition time are evaluated numerically at the interval extremes and at the middle point. At the successive iteration, search exposition interval is reduced to one-half through bisection, selecting the right or left semi-interval basing the choice on first derivative sign evaluated at the middle point and on extremes. The approach proposed is iterated until convergence, which occurs very quickly, thus making the algorithm more efficient with respect to both a very expensive approach based on the subdivision of the domain in a refined grid of points and with recently presented GA procedures.

As well know, in the production process, a wide spread of commercial peroxides may be used, as they could ensure a relatively defined level of vulcanization (in some cases they could also react via addition to double bond producing higher reaction efficiency) of the final product at a given curing temperature. Nevertheless, it is possible that thick rubber items reach an inhomogeneous degree of vulcanization at the end of the industrial process, due to the very different temperature conditions, which undergo external layers with respect to the core. In all these cases, a possibility to improve final mechanical properties is to utilize mixtures of two peroxides, able to vulcanize EPM/EPDM rubber at different temperatures because highly active the first for external layers, the second for the core.

In this article, two examples of technical relevance are analyzed, the first relying in a thick high-voltage electric cables insulator (axi-symmetric case), the second in a thick 3D EPDM dock bumper obtained by compression molding. Only in the latter case, peroxides mixtures are needed to obtain a homogeneous vulcanization, whereas for the first example a sufficient level of vulcanization is obtained even using a single peroxide.

When dealing with the second example, for the sake of conciseness, only a set of mixtures of 2.5-dimethyl-2.5-bis-(t-butylperoxy)-hexane (AkzoNobel Trigonox 101[6] hereafter called Peroxide E) and 1.1 bis (t.butyl-peroxy)-3.3.5 trimetylcyclohexane (AkzoNobel Trigonox 29,[6] hereafter called Peroxide A) is considered. Such peroxides have considerable differences in $t_{1/2}$ at 6 min (0.1 hours), respectively at 171°C and 138°C. Both are usually utilized in practice to vulcanize EPM/EPDM rubber and their marked different behavior seems particularly suited to obtain a homogeneous vulcanization of thick items. Mixing molar ratios considered are 50%-50% 75%-25%, and 25%-75%. Results obtained with the

aforementioned mixing ratios are compared with 0%-100% 100%-0% mixtures, representing vulcanization with only Trigonox 101 and Trigonox 29 respectively.

In both cases, optimal production T_c and t parameters are numerically evaluated with the numerical procedure proposed. Simulations results show that the algorithm proposed is very stable and that optimal production parameters are obtained, for all the cases analyzed, requiring a very limited processing time.

3D RUBBER THICK ELEMENTS VULCANIZATION

Commercial vulcanization of rubber items is obtained almost exclusively by compression (or injection) molding and extrusion.

A number of different elastomers can be cross-linked using peroxides.[9–15] Their utilization is a consequence of their easiness of formation of free radicals. When dealing with EPM/EPDM elastomers, cross-linking occurs by means of common organic peroxides. EPM/EPDM rubber, in fact, is constituted by saturated linear macromolecules with a paraffinic structure, with controlled quantities of insaturations (for EPDM), external to the main chain. As well known, peroxide vulcanization on unsaturated elastomers could also react via addition to double bond and it could produce higher reaction efficiency; hence, different network structure and mechanical properties could be obtained, depending on peroxide and instauration type, temperature, peroxide concentration, etc. Obviously it has not influence on EPM and it is not very important in EPDM and for EPDM with low amount of ENB. The selection of the most appropriate peroxide is a very difficult task, as it is obviously necessary to have a deep knowledge of both the application to which the peroxide is used and the process method, as well as the operating conditions.

The first step in a peroxide-induced vulcanization is the decomposition of the peroxide to give free radicals,[16–19] i.e. peroxide, $\rightarrow 2R^{\bullet}$, where $R^{\bullet}$ is an alkoxil, an alkyl or an acyloxyl radical, depending on the typology of peroxide used.

Peroxides decomposition kinetic is of first order, i.e., $-\frac{dc}{dt} = kC$ where C is the concentration (mol/m^3) of the unreacted peroxide, and k is a kinetic constant for a fixed peroxide.

$C(t)$ is obtained by simply splitting variables (if and only if k does not depend on exposition time), i.e., $C(t)/C_0 = e^{-kt}$, where C_0 is the initial peroxide concentration (all unreacted) and $C(t)$ is the unreacted peroxide concentration at time t. Defining as half-life $t_{1/2}$ the time required to obtain a concentration of unreacted peroxide equal to $C_0/2$, k is equal to $\ln 2/t_{1/2}$.

Therefore, reaction kinetic can be re-written as:

$$\frac{C(t)}{C_0} = \frac{1}{2} e^{\left(1-\frac{t}{t_{1/2}(T)}\right)\ln 2} \tag{1}$$

which describes the absolute decrease of peroxide unreacted concentration at different times with respect to parameter $t_{1/2}$.

As experimental evidences show, the rate of reaction, and hence $t_{1/2}$, is temperature dependent. In Figure 1, for instance, the behavior at different temperatures in terms of $t_{1/2}$ parameter of 30 different commercial peroxides are reported.

Such a dependence is expressed by the classical Arrhenius equation[1,2,4,15]:

$$k(T) = k_{\max} e^{-\frac{E_a}{R_g T}} \tag{2}$$

where $k(T)$ is the peroxide velocity constant at a temperature T, E_a is the so-called energy of activation kJ/mol, R_g is the general gas constant (8.134 J/molK), T is the absolute temperature, $k_{\max}$ is the velocity constant for $T \rightarrow +\infty$.

From eq. (2), it can be proved that:

$$\begin{aligned} t_{1/2}(T_2)/t_{1/2}(T_1) &= e^{-\frac{E_a}{R_g}\left(\frac{1}{T_1}-\frac{1}{T_2}\right)} \\ &\Rightarrow \ln(t_{1/2}(T_2)) - \ln(t_{1/2}(T_1)) \\ &= \frac{E_a}{R_g}\left(\frac{1}{T_1}-\frac{1}{T_2}\right) \end{aligned} \tag{3}$$

where T_1 and T_2 are two generic absolute temperatures.

Law (3) in semi-logarithmic form is commonly used by practitioners to have an idea of the peroxide to use in the manufacturing process. As a rule, engineers know (from their own experience) approximately exposition time and curing temperature T_c. From exposition time, peroxide to use is normally selected multiplying exposition time by 0.3, hence finding $t_{1/2}$ half-life decomposition of the plant. In this way, a restricted number of commercial peroxides are selected. Considering also that the maximum value of the temperature profile for external rubber layers is usually not far from T_c (is equal to T_c for vulcanization by conduction), manufactures experience drives the final choice of the peroxide to use.

Nevertheless, rubber products are usually thick and rubber industries try to solve vulcanization problems (heterogeneous properties caused by the under-vulcanization on the core and over-vulcanization on the skin of the final product) by trial-and-error experiments. Usually these technologies are

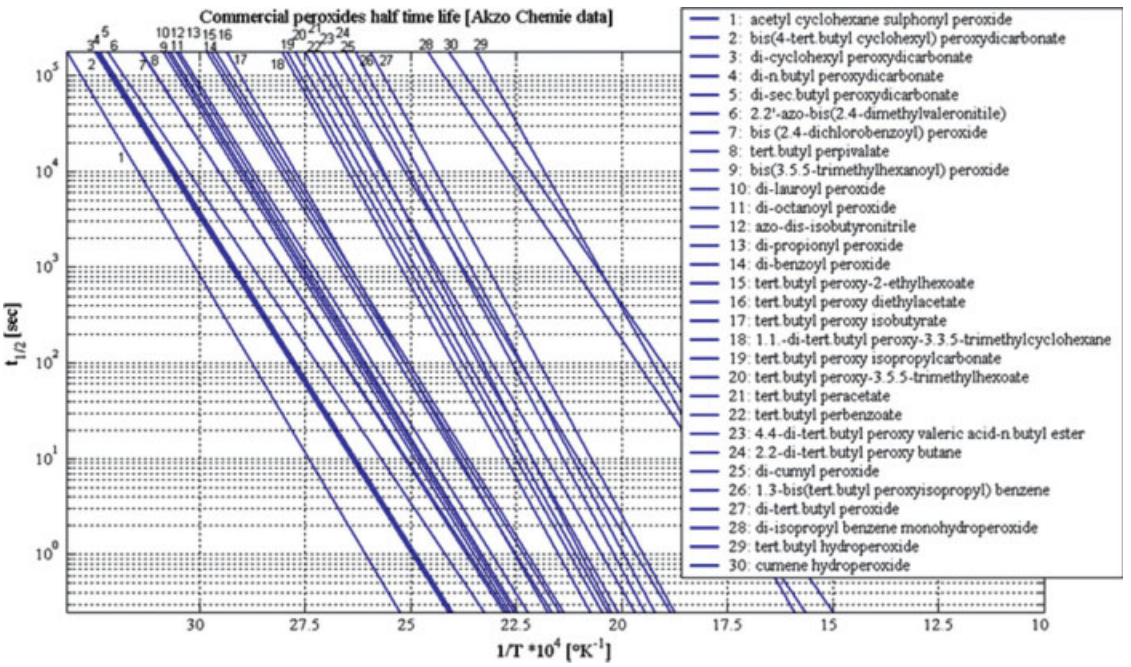

Figure 1 Commercial peroxides temperature $t_{1/2}$ curves. [Color figure can be viewed in the online issue, which is available at www.interscience.wiley.com.]

based on the experience of the specialized workers. It would be therefore particularly useful to establish, by means of a numerical/theoretical model, a double-peroxide mix to use to optimize overall vulcanization. The aim is to activate vulcanization of the cool internal zone with one peroxide, whereas the other is active for the hot coat.

When a total initial concentration C_0 of two peroxides is present in the mixture, we assume that each peroxide decompose separately following a first order differential equation. Indicating with index 1 and 2 peroxide 1 and 2 respectively and with $C = C_1 + C_2$ the sum of peroxides unreacted concentrations, we obtain:

$$\left.\begin{aligned} -\frac{dC_1}{dt} &= k_1 C_1 \\ -\frac{dC_2}{dt} &= k_2 C_2 \end{aligned}\right\} \Rightarrow -\frac{d(C_1 + C_2)}{dt} = k_1 C_1 + k_2 C_2 \qquad (4)$$

Assuming that $C_{10} = \chi C_0$ and $C_{20} = (1 - \chi)C_0$ are initial peroxides concentrations and supposing that each peroxide constant k_i follows Arrhenius equation (2), we obtain:

$$-\frac{d(C/C_0)}{dt} = \chi k_{1\max} e^{\frac{E_{a1}}{R_g T}} \frac{C_1}{C_{10}} + (1 - \chi) k_{2\max} e^{\frac{E_{a2}}{R_g T}} \frac{C_2}{C_{20}} \qquad (5)$$

which gives the variation of total unreacted peroxides concentration with respect to actual concentrations of peroxides.

It is interesting to notice from eqs. (5) and (4) that an integral may be obtained analytically only supposing temperature T constant. Obviously, during vulcanization, $T = T(t)$ and therefore a numerical integration is needed for each point of the items to vulcanize. In particular, an explicit Runge-Kutta (4,5) formula[20] is utilized, needing only the knowledge of the solution at the immediately preceding time point.

Cured rubber tensile strength

Vulcanized rubber and thermoplastic elastomers (TPE) often fail in service due to the generation and propagation of special type of ruptures, called "tear," with elasto-plastic and even fragile phenomena. Other usual failures are those due to the lack of tensile strength. From the aforementioned considerations, it appears particularly interesting to propose an optimization process able to maximize tensile strength σ_t.[21]

From a theoretical and practical point of view, to link the vulcanization process with mechanical properties of rubber is not an easy task. Elasticity and mechanical properties of elastomers depend on the network structure obtained during the vulcanization reaction. Network structure is defined by different parameters such as crosslinking density, distribution of crosslinks and their functionality, entanglements, network defects (loops, dangling chains, etc.). It is possible to assume that the amount of crosslinks is the key-factor that determines the mechanical properties on rubber compounds. Crosslink density depends on the conversion rate of curing agents (in the case of vulcanization with peroxides it is the

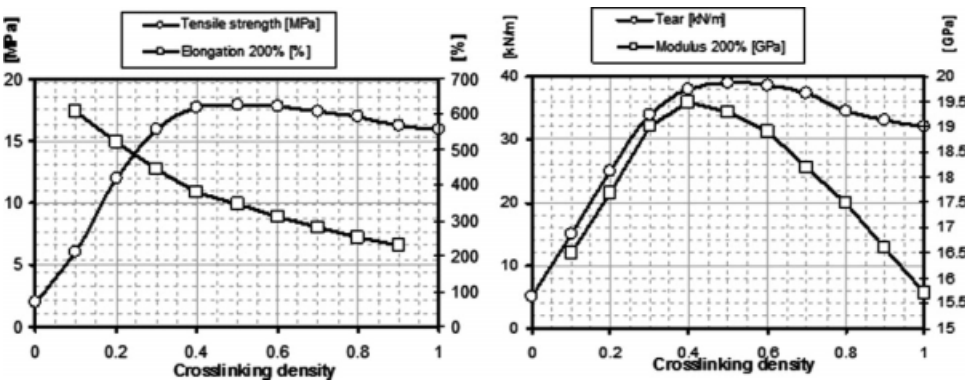

Figure 2 Nonlinear behavior of some output rubber mechanical properties with respect to peroxide unreacted concentration (data processed from Hofmann experimentation[8]).

thermal decomposition of peroxides) at given reactive concentrations. Nevertheless, crosslinking density (hence mechanical properties) depends also on the initial concentration of peroxide. In this article, initial concentrations are set equal to experimental data provided by Hofmann[8] and represent typical values used in the industry. A work in progress by the authors is to change initial concentrations in a wide range, meaning that a new variable has to be handled in the problem, thus making the optimization a very difficult task. Within these hypotheses, at a fixed initial concentration, it can be argued (see also,[8,9,22]) that rubber macroscopic mechanical properties (tear resistance, tensile strength, Young modulus, etc.) depend on C/C_0 ratio, where C is the concentration of unreacted peroxide and C_0 is its initial concentration in the mixture, see Figure 2. As peroxide concentration depends on curing time via half-life $t_{1/2}$ parameter [see eq. (1)] and being $t_{1/2}$ a function of absolute temperature T, rubber macroscopic mechanical properties are dependent on curing time[8] nontrivially. In particular, it has been shown that tensile strength depends on crosslinking density (or curing time) nonmonotonically, that is, maximum is reached at ureacted peroxide concentrations >0, see Figure 3 and Hoffmann.[8]

In Figure 4, rubber behavior vulcanized with peroxide A and peroxide E is shown as a function of temperature and exposition time. In particular, in Figure 4(a,c) tensile strength function is reported, whereas in Figure 4(b,d) unreacted peroxide concentration is plotted as a function of T and t. As it is possible to notice, Figure 4(a,c), optimal tensile strength is reached only at particular values of T and t. Obviously, such a representation is able to give correct information on output parameters only at constant temperatures (note that $T \neq T_c$, being T rubber temperature), that is, results reported in Figure 4 cannot be applied directly to a rubber infinitesimal element subjected to curing, because its temperature changes continuously at successive time steps.

As well known, in fact, real nonconstant temperature profiles $T = T(\mathbf{P},t)$ for each point $\mathbf{P}$ of the element to vulcanize have to be determined solving a suitable differential system, as it will be shown in what follows. Nonetheless, Figure 4 gives technically useful (even approximate) information on the complex behavior of rubber during vulcanization, addressing that a strong variability of output mechanical properties is obtained changing peroxide.

Finally, it is stressed that the numerical procedure presented can be adapted to any parameter chosen as optimization variable and to any peroxide, simply substituting (1) input numerical interpolation functions depicted in Figure 3 and (2) $t_{1/2} - T$ curves.

KERNEL OF THE NUMERICAL MODEL ADOPTED

In this section, the basic features of the numerical approach utilized for the optimization of complex 2D/3D rubber thick elements is outlined.

Essentially, the following blocks are repeated in the code at different T_c or exposition times:

1. Determination of temperature profiles for each point of the item (i.e. node in the FEM mesh).

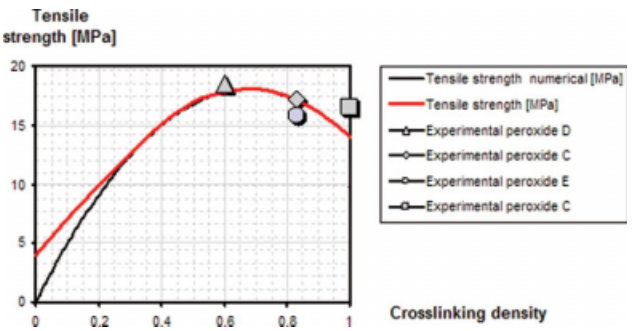

Figure 3 Quadratic interpolation of experimental data, tensile strength-cross-linking density data. [Color figure can be viewed in the online issue, which is available at www.interscience.wiley.com.]

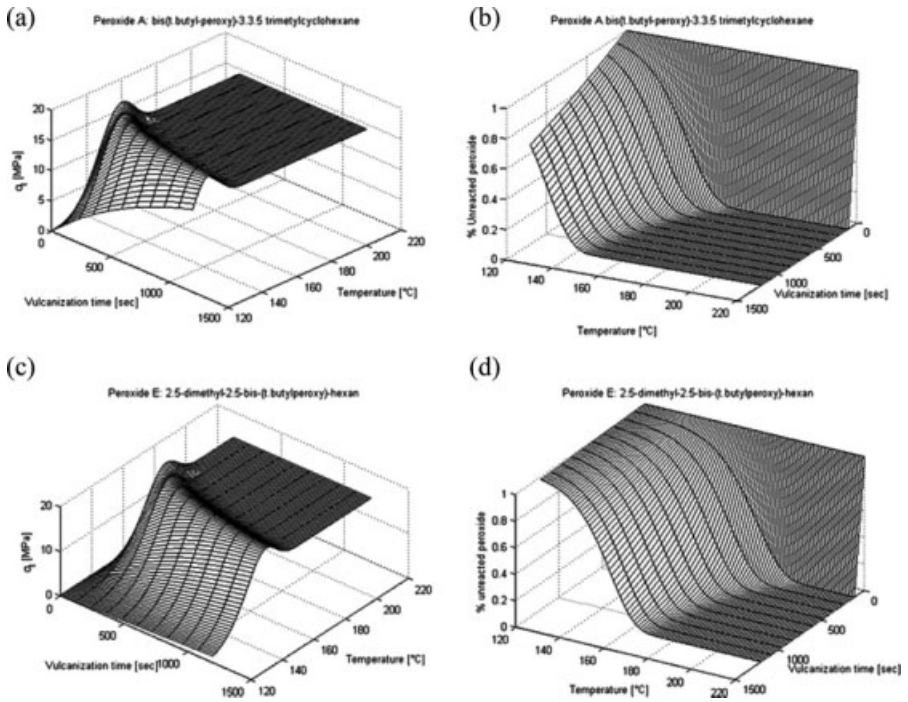

Figure 4 Peroxide A (a and b) and Peroxide E (c and d) behavior during vulcanization. Tensile strength (a and c) and % peroxide unreacted concentration (b and d) at different temperatures and exposition times.

At this aim, heat transmission Fourier's law in 2D/3D dimensions[4,23] is utilized. As in the most general case, Fourier's equation is partial and differential, a finite element (FEM[24]) strategy is implemented to solve the problem.

2. Determination, for each point of the object, of its final mechanical properties at different temperatures and different exposition times. An optimal vulcanization time at different insulator fixed temperatures exists, where objective function (tensile stress, elongation, tear strength, etc.) is maximized. As we are interested in evaluating the overall properties of the vulcanized rubber, an averaged objective function is adopted (i.e. the mean tensile strength is maximized).
3. Determination, by means of a simple alternating tangent (AT) procedure of optimal ($T_{ci}t_i$) input pairs where output mechanical properties are maximized. The AT method requires to proceed through sections in which $T(c)$ or t are fixed, in bounding the remaining undetermined variable at the first iteration, in evaluating tensile strength first derivatives at the extremes and at the middle point of the interval inspected and in bisecting iteratively the interval on the base of first derivative sign.

Governing partial differential equations

The vulcanization process can be schematically subdivided into two separate phases: first, elastomers are exposed to high temperatures in order to activate peroxidic cross-linking and thus vulcanization, followed by a second cooling phase (usually with air or water) in which rubber is kept to ambient temperature.

Temperature profiles for each point of the element are obtained solving numerically a partial differential equations system problem. Fourier's heat equation law is used.[23] In particular, the heat balance field equation is the following:

$$\rho_p c_p^p \left(\frac{\partial T}{\partial t}\right) - \lambda_p \bigtriangledown^2 T - r_p \Delta H_r = 0 \qquad (6)$$

where:

- ρ_p, c_p^p and λ_p are EPDM density, specific heat capacity, and heat conductivity respectively;
- ΔH_r is rubber specific heat (enthalpy) of reaction and is expressed in kJ/mol;
- r_p is the rate of cross-linking and is expressed in mol/(m^{3}sec).

It is worth noting that the term $r_p \Delta H_r$ in eq. (6) is the heat required by the decomposition of the peroxide. ΔH_r, usually ranges from 120 to 180 kJ/mol, representing the bone breaking between oxygen–oxygen in the peroxide. $r_p \Delta H_r$ depends on both T and t and several models can be used for an analytical definition of r_p function. Nonetheless, for the sake of simplicity, we assume here a constant behavior for r_p with respect to concentration time first derivative, i.e., $r_p \propto \frac{dC}{dt}$. More complex relations can

be adopted[4] in the model proposed without any numerical difficulty.

Initial and boundary conditions

Two different boundary conditions are applied when dealing with radiation + convection or conduction.

If heat transmission at the external boundary is due to convection + radiation (extrusion process) the following boundary conditions must be applied:

$$\lambda_p \frac{\partial T(\mathbf{P},t)}{\partial \mathbf{n}(\mathbf{P})} + h(T(\mathbf{P},t) - T_c) + q_{\text{rad}} = 0 \qquad (7)$$

where h is the heat transfer coefficient between EPDM and vulcanizing agent at fixed temperature T_c, $\mathbf{P}$ is a point on the object surface and $\mathbf{n}$ is the outward versor on $\mathbf{P}$, q_{rad} is the heat flux transferred by radiation. Radiation contribution for the vulcanization of complex 3D geometries may not be determined precisely. At a first glance, the simplified following formula is applied:

$$q_{\text{rad}} = \sigma\left(T_c^4 - T\left(R_p,t\right)^4\right) / \left[1/\varepsilon_p + \frac{A_p}{A_c}(1/\varepsilon_c - 1)\right] \qquad (8)$$

where $\sigma = 5.67 \cdot 10^{-8}$ W/m^{2}K^4 the Stefan-Boltzmann constant, $\varepsilon_{p,c}$ are emissivity coefficients, $A_{p,c}$ are the areas of heat exchange (p: insulator, c: curing agent).

When dealing with a compression molding process, the external boundary of the 3D element is subjected to the constant temperature T_c of the steel matrix at increasing time, i.e.,

$$T(\mathbf{P}) = T_c \quad \forall \mathbf{P} \in \partial\Omega \qquad (9)$$

where $\mathbf{P}$ is a point on the boundary surface $\partial\Omega$.

For the cooling phase, no differences occur with respect to the curing process, provided that the temperature of the cooling agent is known at increasing time steps.

Both for extrusion and molding, heat exchange during the cooling phase occurs for convection, i.e. following the partial differential equation:

$$\lambda_p \frac{\partial T(\mathbf{P},t)}{\partial \mathbf{n}(\mathbf{P})} + h_w(T(\mathbf{P},t) - T_w) = 0 \qquad (10)$$

where h_w is the water (air) heat transfer coefficient, T_w is the water (air) cooling temperature and all the other symbols have been already introduced.

Initial conditions on temperatures at each point at the beginning of the curing process are identically equal to the ambient temperature (hereafter fixed equal to 25°C for the sake of simplicity), whereas initial conditions at the beginning of the cooling phase are obtained from the temperature profiles evaluated at the last step of the cooling zone, i.e. at $T(\mathbf{P},t_c)$, where t_c is the total curing time and $\mathbf{P}$ is a generic point belonging to Ω.

Finite element (FE) implementation: Tetrahedrons (3D case) and quadrilateral four-noded elements (2D case)

Partial differential equations system (6-10) for complicated geometries and initial temperatures conditions can not be solved in closed-form. Therefore, in what follows, a Finite Element (FEM)[23–26] discretization of the domain is utilized to obtain a reliable approximation of temperatures at each element point and at successive time steps. The procedure has been completely implemented in Matlab[27] language. In this way, resultant FE temperature profiles at each time step are directly collected from the numerical analysis and utilized for the evaluation of output rubber mechanical properties by means of an integrated tool.

When dealing with 3D rubber objects, tetrahedron four-noded elements have been used. Temperature field interpolation is assumed linear inside each element, i.e.:

$$T(\mathbf{P}) = \mathbf{N}^e\mathbf{T}^e \qquad (11)$$

where $\mathbf{T}^e = [T^1T^2T^3T^4]^T$ is the vector of nodal temperatures, $\mathbf{N}^e = [N^1N^2N^3N^4]$ is the vector of so-called shape functions N^i ($i = 1,\ldots,4$) and $\mathbf{P}$ is a point of coordinates x_p, y_p and z_p.

Indicating with $\mathbf{X}_i = (x_i, y_i, z_i)$ tetrahedron vertices (i.e. nodal) coordinates, N^i are expressed by the following relation:

$$\mathbf{X} = \sum_{i=1}^{4} N_i(\xi_1,\xi_2,\xi_3)\mathbf{X}_i$$

$$N^i = \begin{cases} 1 - \xi_1 - \xi_2 - \xi_3 & i = 1 \\ \xi_{i-1} & i = 2,3,4 \end{cases} \qquad (12)$$

where $\mathbf{X}$ is a point internal to the tetrahedron (coordinates (x y z)), $\xi_i \in [0\ 1]$ is a normalized coordinate and vertices nodes are obtained alternatively imposing $\xi_j = 1$ and $\xi_i = 0$ for $i \neq j$ (except for node $i = 1$ obtained assuming identically $i = 0$).

For 2D items, quadrilateral four-noded elements have been used. In this case, temperature field interpolation is quadratic inside each element, i.e.:

$$T(\mathbf{P}) = \mathbf{N}^e\mathbf{T}^e \qquad (13)$$

with meaning of the symbols analogous to that of eq. (11). In this case, shape functions are expressed by the following equation:

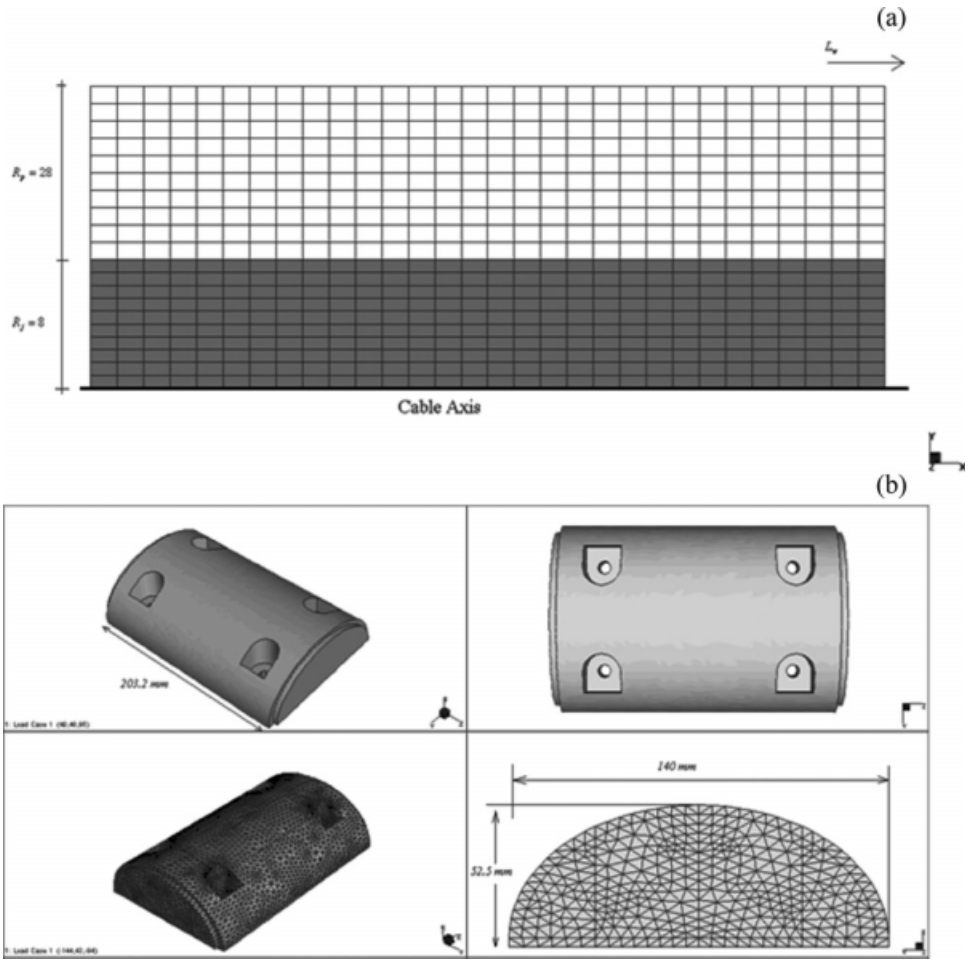

Figure 5 Geometry and FEM discretization by means of (a) four noded quadrilateral elements (high voltage electric cable) and (b) four-noded tetrahedrons of the 2D and 3D items analyzed.

$$N^i(\xi_1, \xi_2) = \frac{1}{4}\left(1 + \xi_1^i \xi_1\right)\left(1 + \xi_2^i \xi_2\right) \quad i = 1, 2, 3, 4 \quad (14)$$

where ξ_1^i and ξ_2^i are the so called "natural coordinates" of node i (ξ_1^i=−1; 1; 1; −1 and ξ_2^i=−1; −1; 1; 1 for $i = 1; 2; 3; 4$ respectively).

In the numerical simulations reported, the following parameters have been used (see Ref. 3,1): EPM/EPDM density ρ_p =922 Kg/m^3, rubber specific heat capacity c_p^p = 2700 J/(kg°C), λ_p = 0.335 W/(m°C), ΔH_r = kJ/mol, water heat transfer coefficient h_w = 1490.70 W/(m^2°C), curing agent heat transfer coefficient h = 900 W/(m^2°C) [only in case of convection and radiation], ε_p = 0.60, ε_c = 0.70, water cooling temperature $T_w = 25$ °C.

Activation energy E_a and $k_{\max}$ depend on the peroxide used, eq. (2), whereas h_w and h should be derived from well known empirical formulas related to laminar/turbulent flow of fluids, see Ref. 4 for details, nevertheless, here characteristic values are used for the sake of simplicity.

Geometries of the 3D (docks bumper) and 2D (electric cable) rubber elements analyzed in this paper are shown in Figure 5. In Figure 6, two temperature color patches at increasing instants referred to the 3D item are reported. As it is possible to notice, internal points remain at a relatively cool temperature (Fig. 6) even at the end of the vulcanization process.

To have an insight into this phenomenon, in Figure 7 temperature patch for the 3D docks bumper (only 1/4 of the mesh is shown) are represented at 6000 and 2500 s, assuming $T_c = 160$°C and highlighting two different nodes with colored dots (one is a node near the external surface, whereas the other belongs to the internal core). In the simulations, a 50%–50% percentage of Peroxide A and E is used.

Temperature-time, residual peroxides concentration vs time and tensile strength diagrams for the two nodes are reported in Figures 8 and 9 respectively, assuming a curing time equal to 4400 seconds.

As it is possible to notice, Point A reaches a good level of vulcanization [Fig. 8(c)], which is also addressed by the residual unreacted concentration of one of the two peroxides [Fig. 8(b)]. On the contrary, Point B results over-vulcanized [Fig. 9(c)], meaning

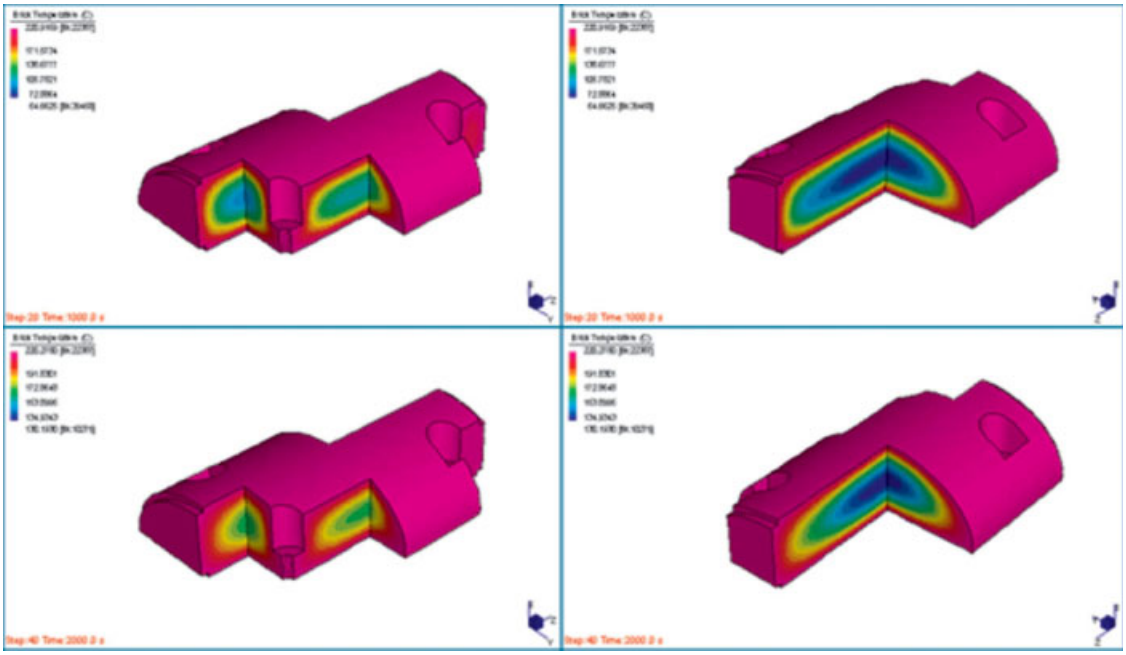

Figure 6 3D docks bumper. Temperatures distribution resulting from the FEM analysis at two different time steps with $T_c = 220°C$. [Color figure can be viewed in the online issue, which is available at www.interscience.wiley.com.]

that both peroxides residual concentration is negligible [Fig. 9(b)]. As one can note, it is particularly evident the difference in the resulting tensile strength at the end of the vulcanization process, a direct consequence of the different temperature profiles of the two nodes [compare Figs. 8(a) and 9(a)]. Form the simulations, it is worth noting the existence of an optimal $t - T$ point at which σ_t reaches its maximum for the node of the mesh under consideration, which corresponds to a specific value of unreacted peroxide concentration in the mixture.

THE ALTERNATING TANGENT APPROACH (AT)

The alternating tangent approach (see also von Solms et al.[28]) used in this paper is based on the numerical evaluation of tensile strength first derivatives with respect to exposition time on several sections at fixed curing temperatures T_c and in the iterated bisection of a determined exposition time search interval.

At a fixed T_c temperature, Figure 10, tensile strength is evaluated on two starting points (points 1

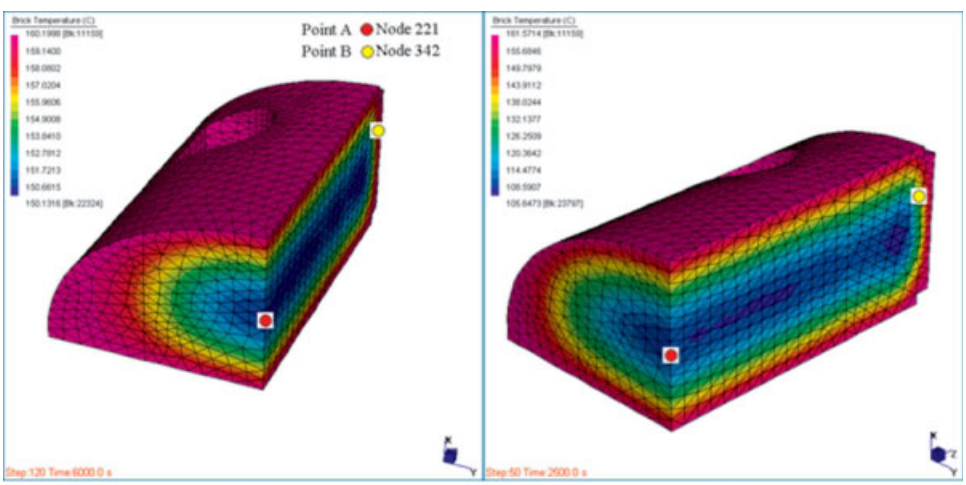

Figure 7 Temperature profile of 3D item at $T_c = 160°C$ and position of nodes inspected (1/4 of the item is shown). (a) 6000 s, (b) 2500 s.

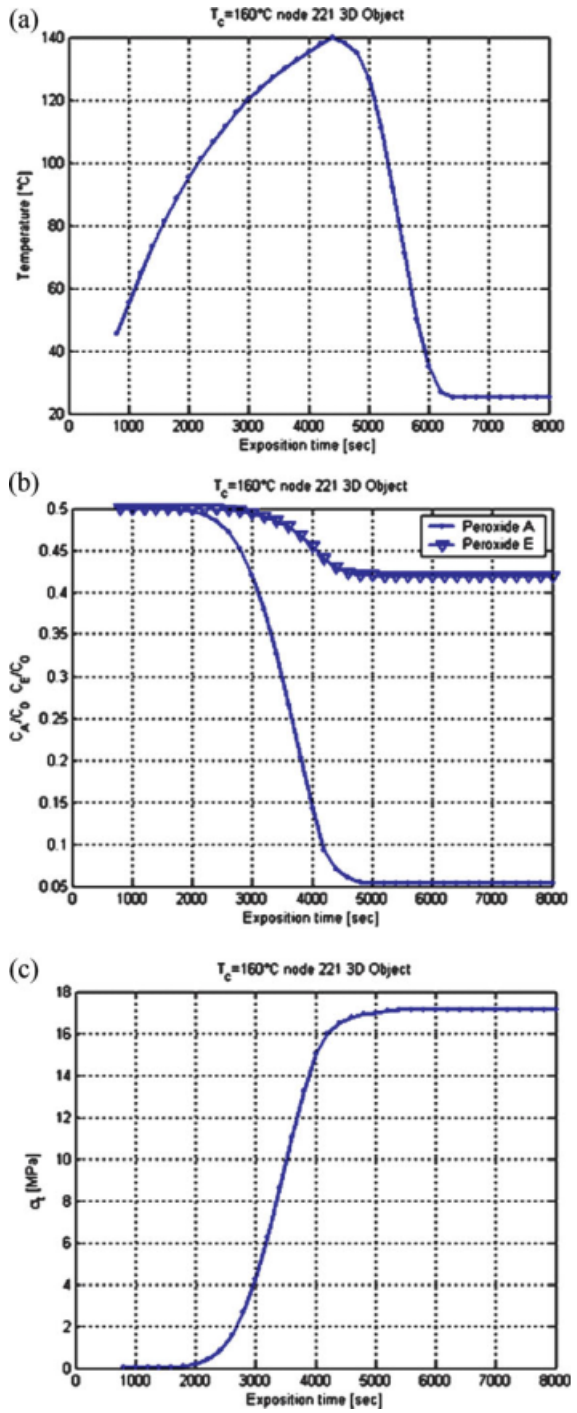

Figure 8 Point A (Node 221, red dot) (a) t -T, (b) t-peroxide concentration and (c) t - σ_t curves. In the case analyzed $\chi = 0.5$. [Color figure can be viewed in the online issue, which is available at www.interscience.wiley.com.]

and 2) called the extremes of the interval search, usually placed at a very under-vulcanized and a very over-vulcanized exposition time (green squares of Fig. 10). Despite the fact that such a choice is fully heuristic, it is sufficient that the over-vulcanized point is set at 5–10 times the value of $t_{1/2}$ of the peroxide used at fixed T_c and the under vulcanized point at 1–5 s, to guarantee that the algorithm does not fail at the preliminary iteration.

First derivatives $d\sigma_t/dt$ of tensile strength with respect to exposition time are needed at the search interval extremes. Since $d\sigma_t/dt$ are not known analytically, a numerical procedure based on finite

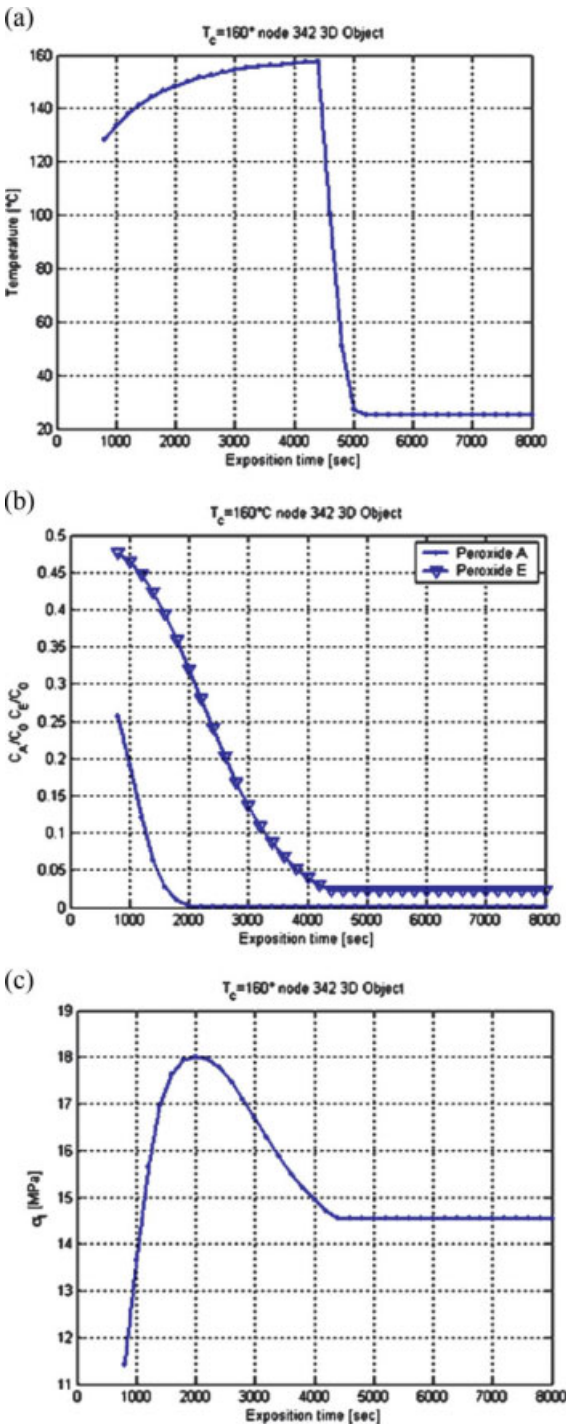

Figure 9 Point B (Node 342, yellow dot) (a) t - T, (b) t-peroxide concentration and (c) t - σ_t curves. In the case analyzed $\chi = 0.5$. [Color figure can be viewed in the online issue, which is available at www.interscience.wiley.com.]

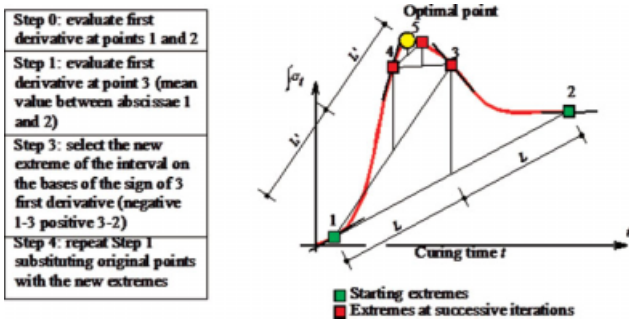

Figure 10 Alternating tangent approach (AT) basic scheme. [Color figure can be viewed in the online issue, which is available at www.interscience.wiley.com.]

differences is adopted. In particular, let 1′ be a point with exposition time equal to 1 plus a small increment Δt and 2′ a point with exposition time equal to 2 decremented of a small Δt.

By definition, numerical first derivative at points 1 and 2 is given by the following equation:

$$\left.\frac{d\sigma_t}{dt}\right|_1 = \frac{\sigma_t|_{1'} - \sigma_t|_1}{\Delta t} \qquad \left.\frac{d\sigma_t}{dt}\right|_2 = \frac{\sigma_t|_2 - \sigma_t|_{2'}}{\Delta t} \tag{15}$$

where the symbol $x\,|_i$ indicates that the quantity x is numerically evaluated at point i.

Authors experienced that a numerically accurate evaluation of first derivatives is obtained fixing Δt in the range 1–3 seconds.

Middle point first derivative of the search interval is also needed, as depicted in Figure 10 (red square, point 3).

Once that first derivatives are at disposal on the search interval extremes and on the middle point, a bisection procedure is adopted, reducing the search interval to one-half. In particular, the new interval is respectively the right or the left one-half depending on the sign of first derivatives of the extremes with respect to the middle point one. More in detail, the following "if statement" is adopted in the algorithm:

$$\begin{aligned} &\text{if } \left.\frac{d\sigma_t}{dt}\right|_1 \cdot \left.\frac{d\sigma_t}{dt}\right|_3 \geq 0 \rightarrow \text{right semi} - \text{interval} \\ &\text{if } \left.\frac{d\sigma_t}{dt}\right|_2 \cdot \left.\frac{d\sigma_t}{dt}\right|_3 \geq 0 \rightarrow \text{left semi} - \text{interval} \end{aligned} \tag{16}$$

The application (16) allows to reduce search interval by one-half. The procedure is repeated on the new reduced interval, until a desired degree of accuracy is obtained (yellow circle in Fig. 10).

It is worth noting that the procedure proposed converges also at fixed exposition times and varying nitrogen temperature T_c, therefore numerical simulations can be performed using two "perpendicular" different strategies (as it will be shown in the numerical simulations reported in the following section).

As a rule, the algorithm converges after few iterations (5–7) to the optimal solution, meaning that the procedure proposed may be used by practitioners instead of more expensive approaches, as for instance the so called grid method (a subdivision of the domain into a regular grid of point in which output tensile strength is evaluated point by point) and GA approaches.[1,2]

NUMERICAL SIMULATIONS

Two sets of numerical simulations are reported in this section, in order to show the capabilities of the alternating tangent approach proposed. In the first example, a two dimensional problem relying in a high voltage electric cable insulator (relatively thick) obtained by extrusion is considered [Fig. 5(a)], whereas in the second example the 3D object of Figure 5(b) is analyzed.

Optimal input parameters functions $\hat{T} = \hat{T}(T_c, t) = 0 \,|\, \hat{T} \equiv \{P^i = (T_c^i, t^i)\text{optimal}\}$ are obtained by means of the AT approach proposed.

In particular, optimal $\hat{T}$ curves (expressed as implicit functions in T_c and t) are numerically evaluated solving the following optimization problem through bisection, once that one of the input parameters T_c^i or t^i is *a priori* fixed (sectional approach):

$$\max \frac{1}{N_L}\sum_{k=1}^{N_L} \sigma_t^k(T_c^i, t^i) \qquad \text{subject to} \begin{cases} T_c^i = \text{fixed} \\ t^{\min} < t^i < t^{\max} \end{cases} \tag{17}$$

$$\text{PDEs system} \begin{cases} \rho_p c_p^p \left(\frac{\partial T}{\partial t}\right) - \lambda_p \nabla^2 T - r_p \Delta H_r = 0 \\ \text{boundary and initial conditions} \end{cases}$$

where N_L is the number of nodes in which the item is discretized and $t^{\min}$ ($t^{\max}$) is a lower (upper) bound limitation for curing temperature.

Results provided by the alternating tangent approach proposed are compared with those obtained subdividing $T_c - t$ plane with a regular grid. In the latter case, for each point $P^{i,j} \equiv (T_c^i, t^j)$ of the grid a mixed algebraic-PDEs system has to be solved:

$$\sigma_t = \frac{1}{N_L}\sum_{k=1}^{N_L} \sigma_t^k(T_c^i, t^j)$$

$$\text{PDEs system} \begin{cases} \rho_p c_p^p \left(\frac{\partial T}{\partial t}\right) - \lambda_p \nabla^2 T - r_p \Delta H_r = 0 \\ \text{boundary and initial conditions} \end{cases} \tag{18}$$

Obviously a very large computational effort is required in solving problem (18), especially for very

refined discretizations (as those needed in the present simulations) using the grid method (otherwise a global optimization algorithm where objective function is not analytically known has to be performed).

The optimization of the high voltage electric cable insulator is obtained by means of three different peroxides. Process starts in an extruder (1), where the conductor (Al or Cu) is coated with the extruded EPM/EPDM. Then the cable enters the heating zone (2), filled with high pressure and high temperature nitrogen (i.e. $T_c \equiv T_n$). Finally, the cable is cooled to the ambient temperature in two steps: in the first step (3), cold water at around 10 bar pressure is used, finally the cable is leaved and cooled in the surrounding air by free convection (4).

During the continuous process, in the curing tube the heat is transferred by convection and radiation from the tube wall through nitrogen to the cable surface, whereas in the cooling zone with water only convection plays an important role (see for instance[4,5]). Usually, the vulcanization tube length for CCV lines can be up to 150 meters (usually 60–80 meters).

For what concerns cables dimensions, we refer to typical insulators thicknesses used by Italian Railways.[29] Italian Railways[29] recommendations to subsuppliers establish the following ranges to adopt for high voltage cables: insulator thickness 10.8–20 mm, conductor diameter 16–38.4 mm, PVC external layer thickness 2.4–4 mm. Within this ranges, the following parameters have been used in the simulations: $R_p = 28$ mm, $R_j = 8$ mm, nitrogen temperature $T_c = 200°C$, water cooling temperature $T_w = 25°C$, length of the heating phase $L_h = 1/2\ L_w = 40$ m.

In Figure 11, rubber mean tensile strength at different temperatures and exposition times is reported for high voltage cables, assuming as reticulation inducer di-cumyl-peroxide. The 3D surface is obtained with an expensive regular grid of points obtained solving (18), whereas yellow circles represent the optimal point obtained with the AT approach. Red squares represent successive intervals extremes, whereas green squares the initial intervals. As it is possible to notice, the algorithm proposed is able to reach tensile maximum strength with sufficient accuracy for all the simulations performed. In this case, simulations are performed fixing exposition time and bisecting curing temperature.

In Figure 12, results for two fixed curing temperatures and varying exposition time are reported. The continuous curve is an expensive section obtained with the grid method, with a grid of 10,000×10000 points. A very refined grid is needed because peaks may be very narrow. Yellow circles and red/green squares are AT iterated solutions.

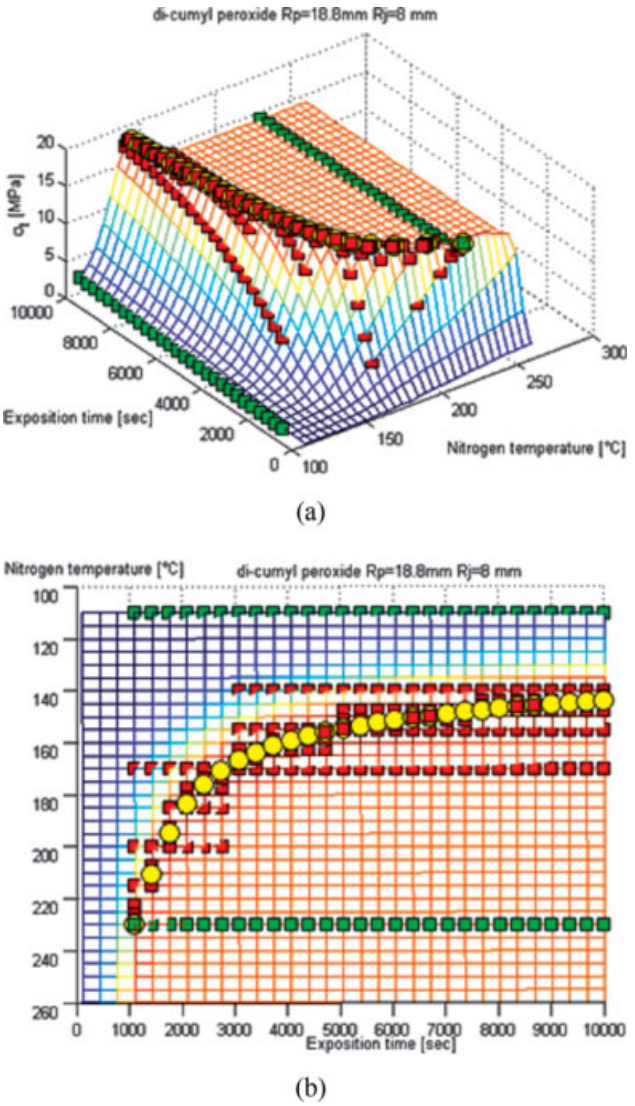

Figure 11 High voltage power cables insulator vulcanized with di-cumyl-peroxide. Optimal output tensile strength at different values of exposition time and nitrogen temperature. (a) 3D view. The surface represents results from the grid method, whereas red/green squares and yellow circles represent AT approach results. Yellow circles are final optimized points form AT approach, red squares extremes of the successive intervals inspected, green squares initial search intervals. (b) aerial view of optimized results. [Color figure can be viewed in the online issue, which is available at www.interscience.wiley.com.]

Simulations are repeated from Figures 13 to 16 using Peroxide A (Figs. 13 and 14) and Peroxide E (Figs. 15 and 16).

As a matter of fact, due to the insulator thickness, considerable differences on the temperature profiles along cable thickness can be found.

A detailed comparison among all the results underlines that peroxide choice is crucial. Each peroxide, in fact, has a different $t_{1/2}(T) - t$ behavior and, in some cases, such characteristic curves are

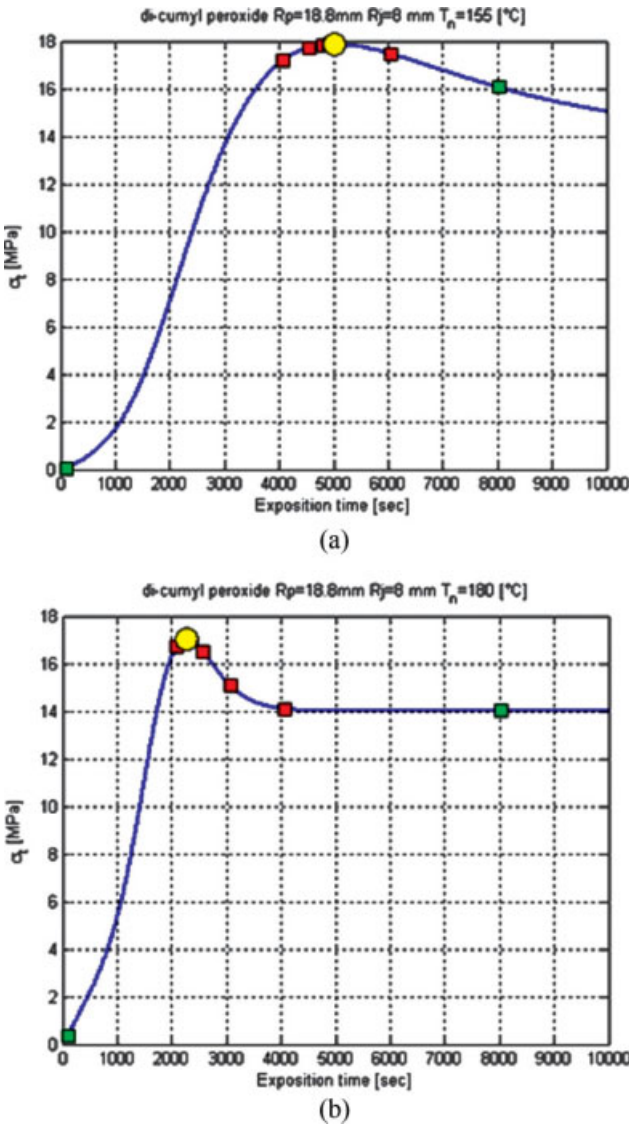

Figure 12 High voltage power cables insulator vulcanized with di-cumyl-peroxide. Optimal output tensile strength at different values of exposition time and fixed value of nitrogen temperature. (a) $T_n = 155°C$. (b) $T_n = 180°C$. The blue line represents results from the grid method, whereas red/green squares and yellow circles represent AT approach results. Yellow circles are final optimized points form AT approach, red squares extremes of the successive intervals inspected, green squares initial search intervals. [Color figure can be viewed in the online issue, which is available at www.interscience.wiley.com.]

sensibly different (see for instance Figs. 11, 13 and 15), resulting in completely different optimal curves for the production line.

The technical usefulness of Figure 11, Figures 13 and 15 is worth noting. In particular, once that a peroxide is chosen, producers can enter in the figures with a desired nitrogen temperature (exposition time) and exit with the optimal exposition time (nitrogen temperature) for the production line. Analogously, *abaci* can be used for the opposite aim to determine the most suitable peroxide to use, once that nitrogen temperature and exposition time are known.

When dealing with the 3D simulations, different % mixtures of Trigonox 101 (peroxide E) and Trigonox 29 (peroxide A) have been chosen to vulcanize uniformly core and skin.

In figures from Figures 17 to 21, tensile strength at different external curing temperatures as a function of exposition time have been reported for five different mixtures of peroxides A and E (peroxide A only, 75% A and 25% E, 50% A and 50% E, 25% A and 75% E, peroxide E only).

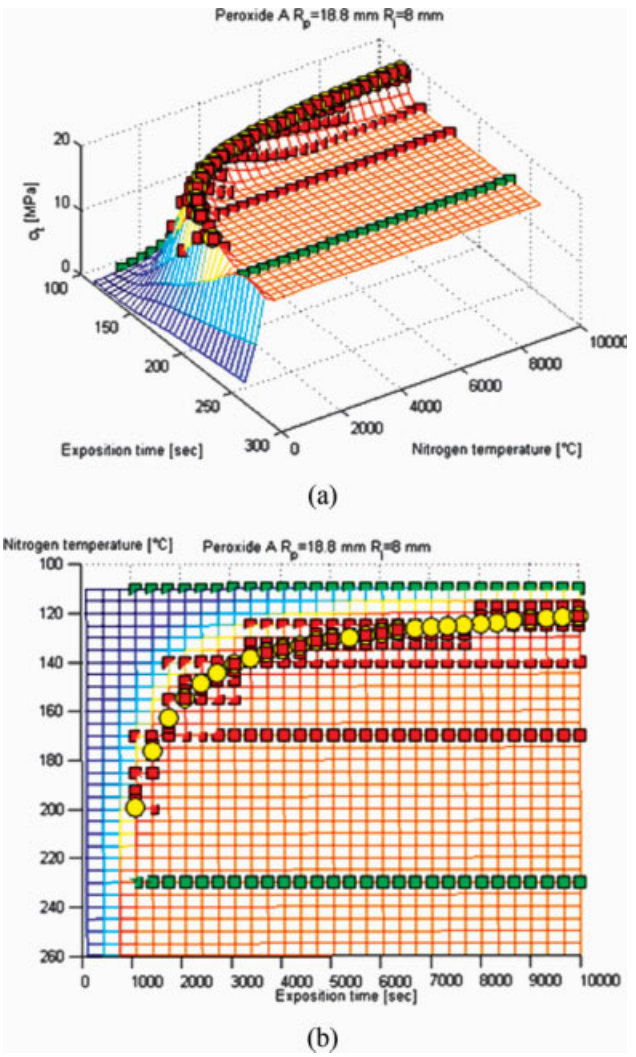

Figure 13 High voltage power cables insulator vulcanized with peroxide A. Optimal output tensile strength at different values of exposition time and nitrogen temperature. (a) 3D view. The surface represents results from the grid method, whereas red/green squares and yellow circles represent AT approach results. Yellow circles are final optimized points form AT approach, red squares extremes of the successive intervals inspected, green squares initial search intervals. (b) Aerial view of optimized results. [Color figure can be viewed in the online issue, which is available at www.interscience.wiley.com.]

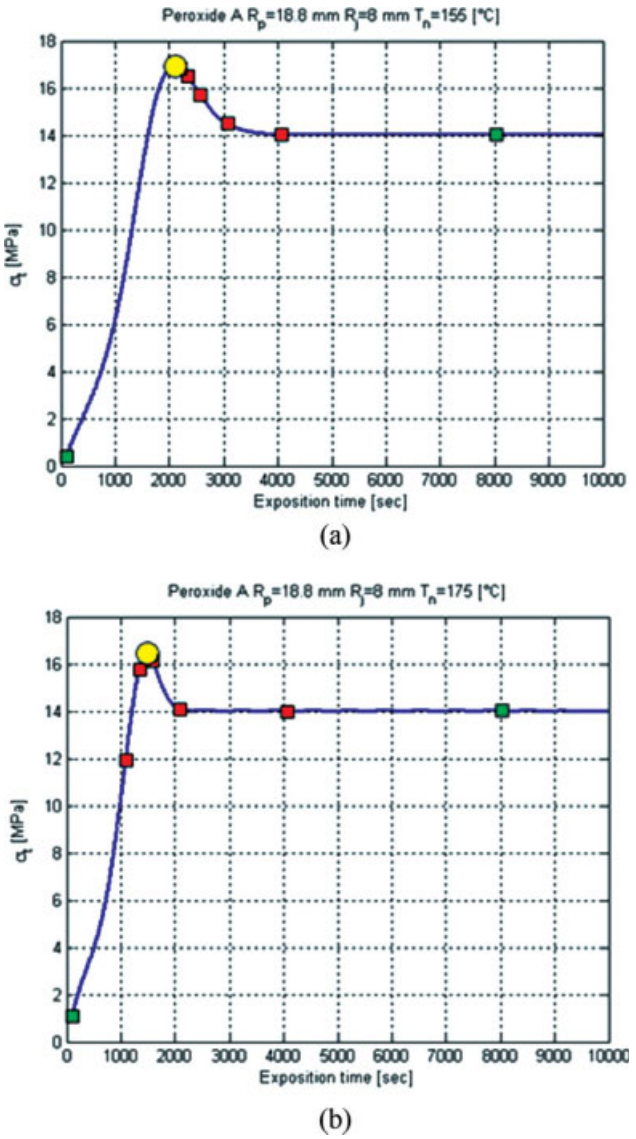

Figure 14 High voltage power cables insulator vulcanized with peroxide A. Optimal output tensile strength at different values of exposition time and fixed value of nitrogen temperature. (a) $T_n = 155°C$. (b) $T_n = 175°C$. The blue line represents results from the grid method, whereas red/green squares and yellow circles represent AT approach results. Yellow circles are final optimized points form AT approach, red squares extremes of the successive intervals inspected, green squares initial search intervals. [Color figure can be viewed in the online issue, which is available at www.interscience.wiley.com.]

For all the cases analyzed, optimization points obtained at each iteration with the AT approach have been compared with those found using a very expensive grid method (each point of the grid required a processing time exceeding 1 h and 15 minutes). Yellow circles in the diagrams represent AT optimized results, whereas red squares the successive extremes of the range inspected during optimization. As it is possible to notice from all the figures, optimal output tensile strength value is reached with the approach proposed for each case analyzed after very few iterations (7–9), whereas a grid with 500 (exposition time) $\times$ 5 (curing temperature) points has been used within the grid method. A less refined grid along exposition time was used in the figures only for the sake of clearness.

Apart the numerical efficiency of the algorithm, from the 3D simulations, it can be deduced that the best results are achieved with a mixture of peroxides at 50%–50% molar ratio, for all the external curing agent temperatures inspected. As can be noticed

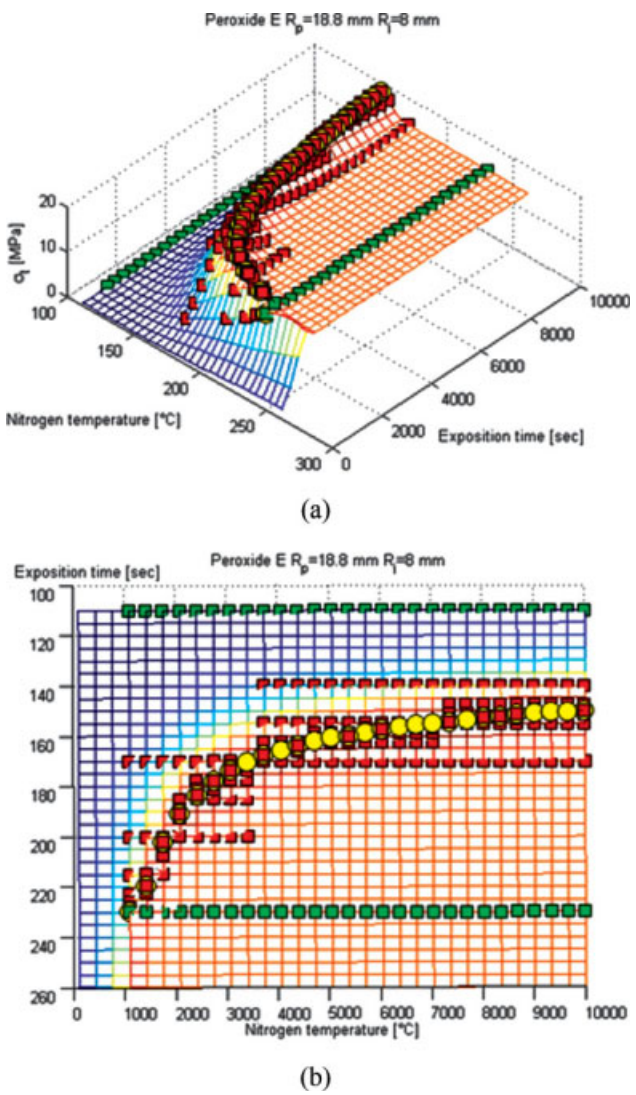

Figure 15 High voltage power cables insulator vulcanized with peroxide E. Optimal output tensile strength at different values of exposition time and nitrogen temperature. (a) 3D view. The surface represents results from the grid method, whereas red/green squares and yellow circles represent AT approach results. Yellow circles are final optimized points form AT approach, red squares extremes of the successive intervals inspected, green squares initial search intervals. (b) Aerial view of optimized results. [Color figure can be viewed in the online issue, which is available at www.interscience.wiley.com.]

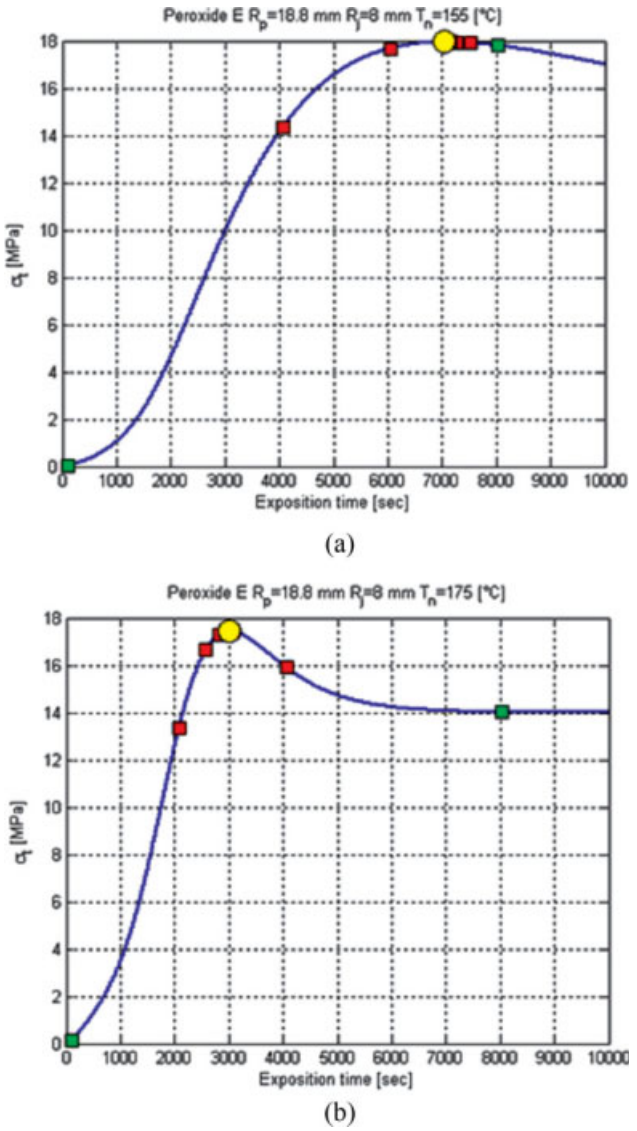

Figure 16 High voltage power cables insulator vulcanized with peroxide E. Optimal output tensile strength at different values of exposition time and fixed value of nitrogen temperature. (a) $T_n = 155°C$. (b) $T_n = 175°C$. The blue line represents results from the grid method, whereas red/green squares and yellow circles represent AT approach results. Yellow circles are final optimized points form AT approach, red squares extremes of the successive intervals inspected, green squares initial search intervals. [Color figure can be viewed in the online issue, which is available at www.interscience.wiley.com.]

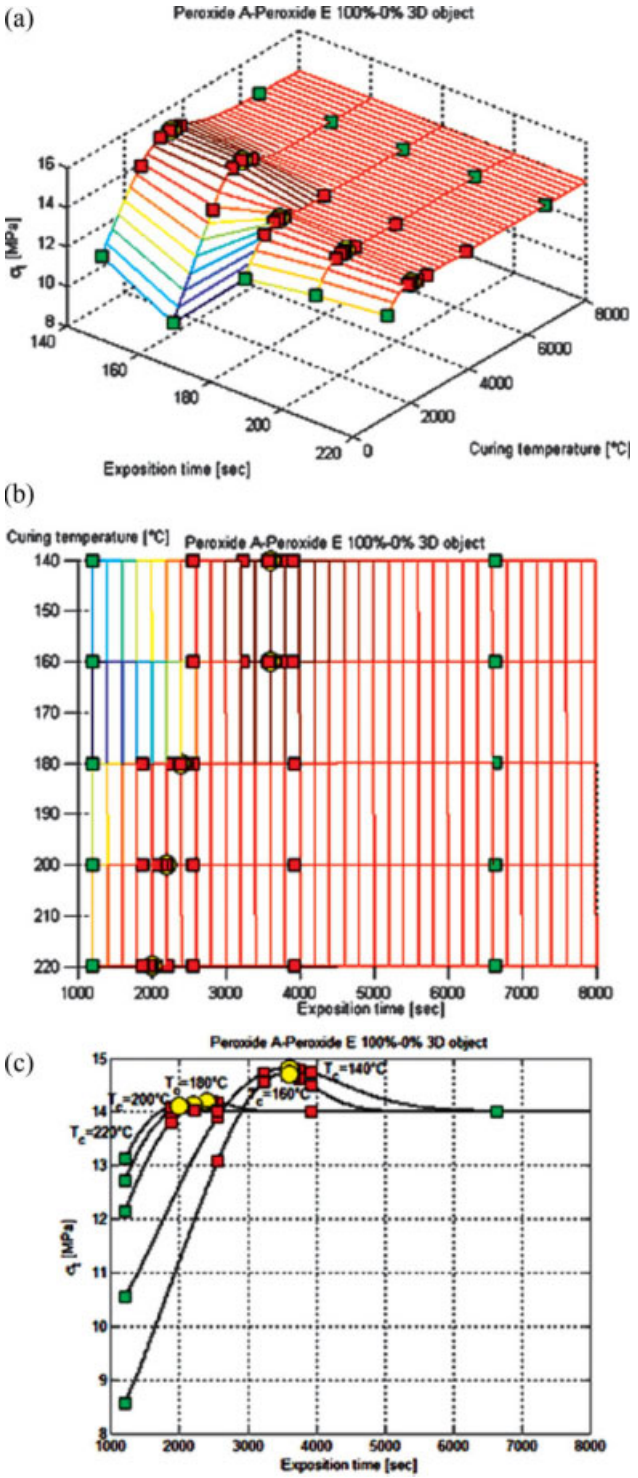

Figure 17 3D item vulcanized with mixture of peroxides (100%–0%). Optimal output tensile strength at different values of exposition time and T_c (a) 3D view. The surface represents results from the grid method, whereas red/green squares and yellow circles represent AT approach results. Yellow circles are final optimized points form AT approach, red squares extremes of the successive intervals inspected, green squares initial search intervals. (b) Aerial view of optimized results. (c) sections at fixed T_c. [Color figure can be viewed in the online issue, which is available at www.interscience.wiley.com.]

from the simulations, the range of optimal temperatures is approximately between 150°C and 160°C. Exceeded 160°, it is yet possible to find optimal values of exposition time, but with a resultant optimized tensile strength which is not sensibly improved with respect to the asymptotic value (i.e., obtained with an over-vulcanization of the item). Such behavior is due to the fact that, at relatively high temperatures of vulcanization, $t_{1/2}$ values of both peroxides reduce considerably. As a

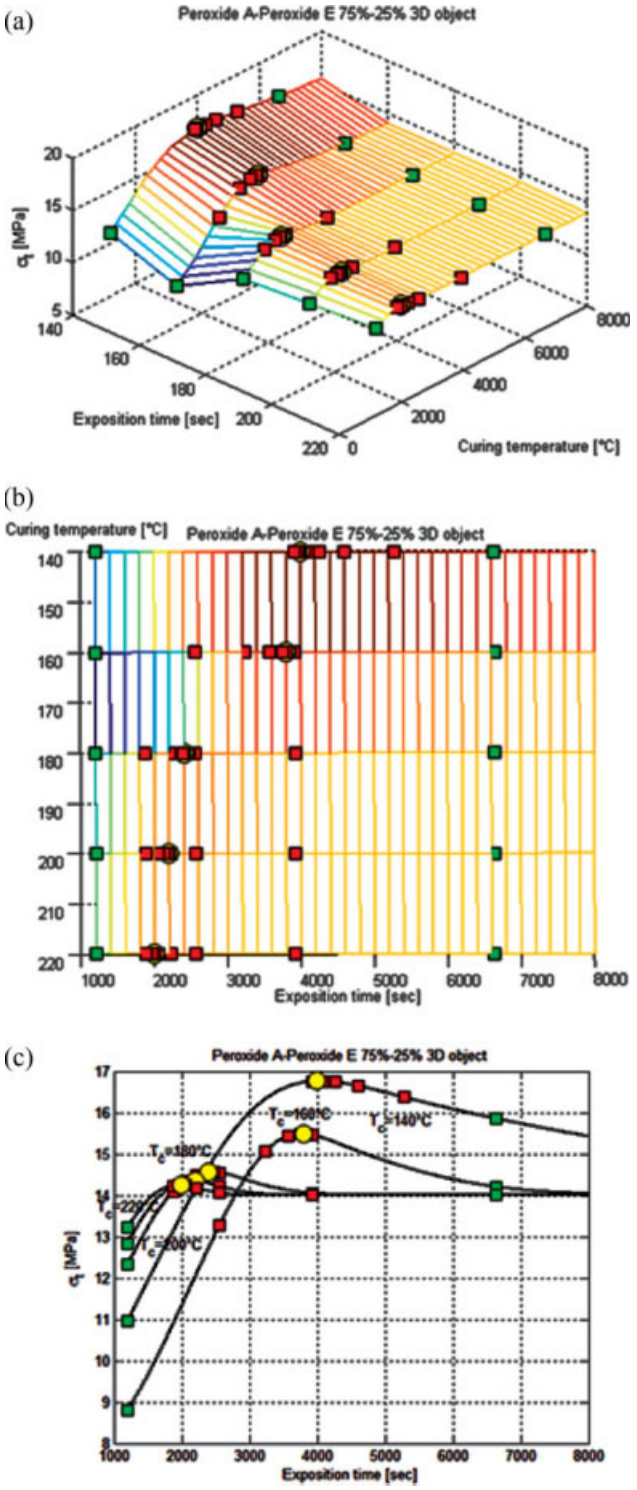

Figure 18 3D item vulcanized with mixture of peroxides (75%–25%). Optimal output tensile strength at different values of exposition time and T_c. (a) 3D view. The surface represents results from the grid method, whereas red/green squares and yellow circles represent AT approach results. Yellow circles are final optimized points form AT approach, red squares extremes of the successive intervals inspected, green squares initial search intervals. (b) Aerial view of optimized results. (c) Sections at fixed T_c. [Color figure can be viewed in the online issue, which is available at www.interscience.wiley.com.]

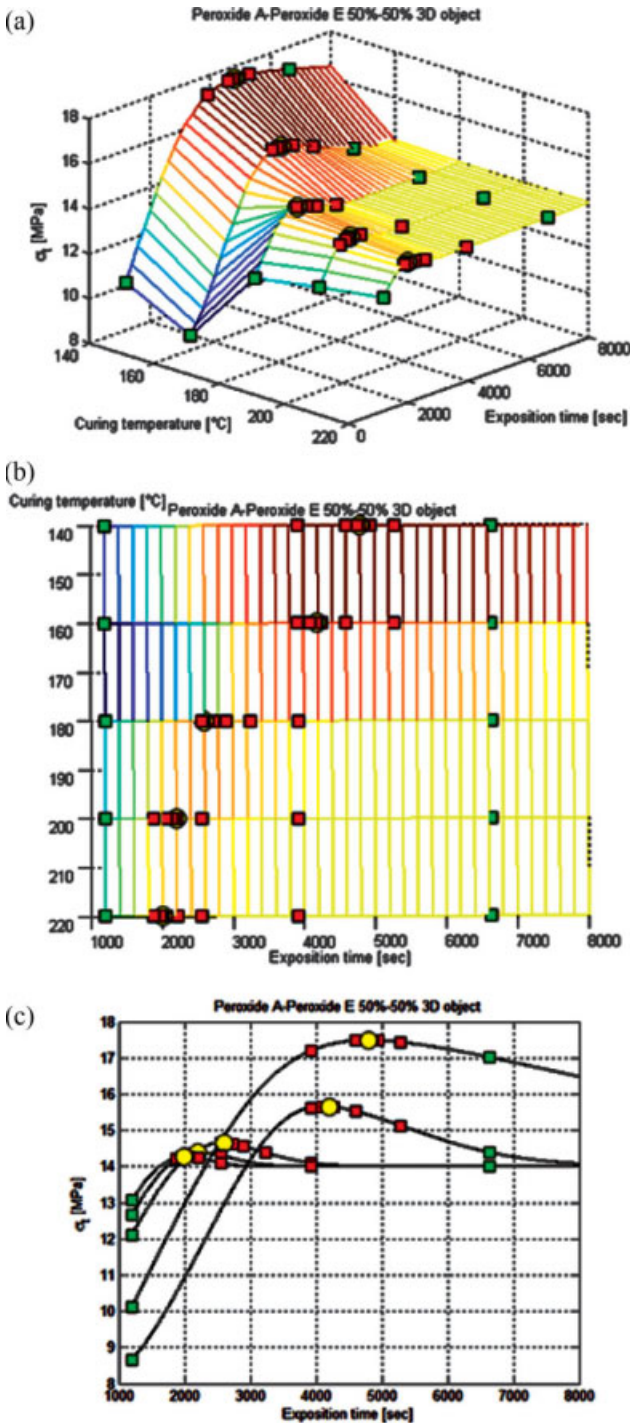

Figure 19 3D item vulcanized with mixture of peroxides (50%–50%). Optimal output tensile strength at different values of exposition time and T_c. (a) 3D view. The surface represents results from the grid method, whereas red/green squares and yellow circles represent AT approach results. Yellow circles are final optimized points form AT approach, red squares extremes of the successive intervals inspected, green squares initial search intervals. (b) Aerial view of optimized results. (c) sections at fixed T_c. [Color figure can be viewed in the online issue, which is available at www.interscience.wiley.com.]

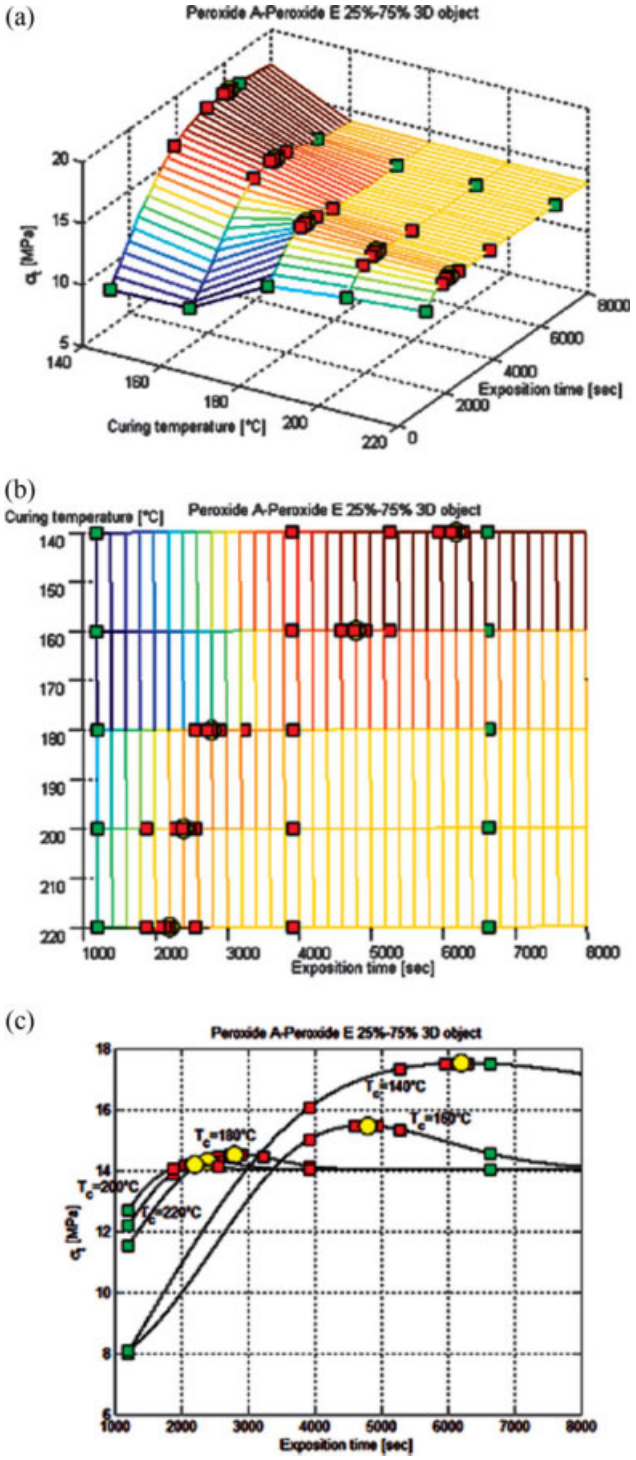

Figure 20 3D item vulcanized with mixture of peroxides (25%–75%). Optimal output tensile strength at different values of exposition time and T_c. (a) 3D view. The surface represents results from the grid method, whereas red/green squares and yellow circles represent AT approach results. Yellow circles are final optimized points form AT approach, red squares extremes of the successive intervals inspected, green squares initial search intervals. (b) Aerial view of optimized results. (c) sections at fixed T_c. [Color figure can be viewed in the online issue, which is available at www.interscience.wiley.com.]

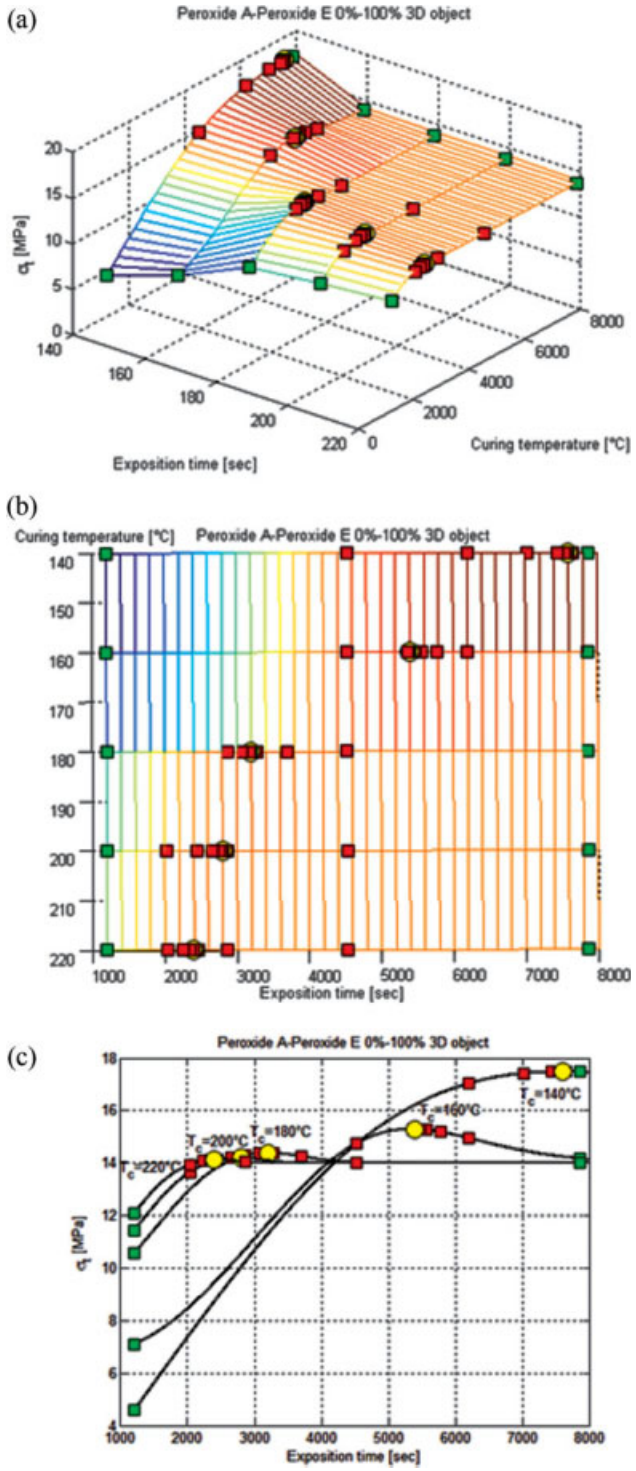

Figure 21 3D item vulcanized with mixture of peroxides (0%-100%). Optimal output tensile strength at different values of exposition time and T_c. (a) 3D view. The surface represents results from the grid method, whereas red/green squares and yellow circles represent AT approach results. Yellow circles are final optimized points form AT approach, red squares extremes of the successive intervals inspected, green squares initial search intervals. (b) Aerial view of optimized results. (c) sections at fixed T_c. [Color figure can be viewed in the online issue, which is available at www.interscience.wiley.com.]

consequence, external layers vulcanization time decreases sensibly, whereas internal core (which, remaining cooler, does not undergo the same temperature profile of the external coat) remains essentially under-vulcanized. Therefore, the peak of the optimal average tensile strength results less marked. In any case, simulations show that peroxides mixtures may improve vulcanization quality in terms of (a) optimal value of tensile strength reached and of (b) reduction of time required for the vulcanization.

CONCLUSIONS

A numerical procedure for the determination of optimal input parameters (curing temperature and exposition time) for 2D/3D thick EPM/EPDM items, eventually in presence of different mixtures of peroxides has been presented. Vulcanization external temperature T_c, rubber exposition time t and different peroxides have been assumed as production parameters to optimize.

Objective function is represented by rubber final mean tensile strength after vulcanization. Despite the fact that the analyzes presented are limited only to the utilization of two input variables and one output mechanical property, the algorithm proposed can be applied without any conceptual difficulty in a more general framework. Furthermore, the same mathematical approach presented can be extended for other polymeric systems that can be vulcanized by peroxides.

The algorithm adopted is a so-called alternating tangent approach (AT). At fixed exposition time (or curing temperature), the remaining input variable has been bounded in the under and over vulcanized region. Resultant tensile strength with its first derivative has been evaluated on the interval extremes and at the middle point. Depending on the sign of such derivatives, a bisectional approach has been adopted to reduce the search interval to one-half. The procedure has been iterated until a desired accuracy of the optimized point was reached.

Two meaningful examples of engineering interest, consisting of a 3D thick rubber docks bumper and an extruded (2D) high voltage cable have been illustrated. For the 3D item, it was necessary to use different mixtures (e.g. 50%-50%, 25%-75%, and 75%-25%) of two peroxides to improve vulcanization quality.

For all the cases analyzed, the efficiency of the numerical procedure proposed has been demonstrated.

References

1. Milani, G.; Milani, F. Comput Chem Eng 2008, 32, 3198.
2. Milani, G.; Milani, F. J Appl Polym Sci 2009, 111, 482.
3. Seymour, D. C.; Krick, D. J Elastomers Plast 1979, 11, 97.
4. Kosar, V.; Gomzi, Z. Thermochim Acta 2007, 457, 70.
5. Kosar, V.; Gomzi, Z.; Sintic, K. Chem Eng Process 2007, 46, 83.
6. AkzoNobel Corporate. Brands and Products Specifications Manual; AkzoNobel Corporate: Amsterdam, The Netherlands, 2008.
7. Bateman, L., Ed. The Chemistry and Physics of Rubber-Like Substances, MacLaren: London, 1963.
8. Hofmann, W. Kautsch Gummi Kunstst 1987, 4.
9. Coran, A. Y. In Science and Technology of Rubber; Frederick, R., Ed. Academic Press: New York, 1978; Chapter 7, pp 291–338.
10. Morton, M., Ed. Rubber Technology, 2nd ed.; Van Nostrand Reinhold: New York, 1981.
11. Drake, R. E.; Labriola, J. M.; Holliday, J. J. Improving Properties of EPM and EPDM with Coagents; American Chemical Society: Chicago, IL, 1994.
12. Drake, R. E.; Labriola, J. M.; Holliday, J. J. 1,2 Polybutadiene Coagents for Improved Elastomeric Properties; American Chemical Society: Nashville, TN, 1992.
13. Roberts, B. E.; Verne, S. Plastic Rubber Process Appl 1984, 4, 135.
14. Di Giulio, E.; Ballini, G. Kautsch Gummi Kunstst 1962, 15, 6.
15. Liu, J.; Yu, W.; Zhao, C.; Zhou, C. Polymer 2007, 48, 2882.
16. Trotman-Dickinson, A. F. J Chem Educ 1969, 46, 396.
17. Scanlan, J.; Thomas, D. K. J Polym Sci Part A: Gen Pap 1963, 1, 1015.
18. Baldwin, F. P.; Ver Strate, G. Rubber Chem Technol 1972, 45, 709.
19. In Encyclopaedia of Polymer Science and Technology; Mark, H. F., Gaylord, N. G.; Bikales, N. M.; Eds.; Wiley: NewYork, 1966; Vol. 4, p 332.
20. Dormand, J. R.; Prince, P. J. J Comp Appl Math 1980, 6, 19.
21. ASTM D412. Standard Test Methods for Vulcanized Rubber and Thermoplastic Elastomers-Tension; American Society for Testing and Materials: Easton, Maryland, 1986.
22. Billmeier, F. W. Jr. Textbook of Polymer Science, 3rd ed.; Wiley: New York, Chichester, Brisbane, Toronto, Singapore, 1984.
23. Evans, G.; Blackledge, J.; Yardley, P. Numerical Methods for Partial Differential Equations, 2nd ed.; Springer-Verlag: Berlin, 2001.
24. Zienkiewicz, O. C.; Taylor, R. L. The Finite Element Method. Vol. I: Basic Formulations and Linear Problems; McGraw-Hill: London, 1989.
25. Jia, Y.; Sun, S.; Xue, S.; Liu, L.; Zhao, G. Polymer 2003, 44, 319.
26. Jia, Y.; Sun, S.; Xue, S.; Liu, L.; Zhao, G. Polymer 2002, 43, 7515.
27. Matlab User's Guide2007. Available at: http://www.mathworks.com/products/matlab/.
28. Von Solms, N.; Kouskoumvekaki, I. A.; Lindvig, T.; Michelsen, M. L.; Kontogeorgis, G. M. Fluid Phase Equilib 2004, 222/223, 87.
29. Italian Railways (FS, Ferrovie dello Stato). Technical Specifications for Medium and High Voltage Cables, 1999, http://site.rfi.it/quadronormativo/Inserimenti.htm